JOURNAL OF MATERIALS SCIENCE 16 (1981) 2419–2433

Production of metallic glass ribbons by the chill-block melt-spinning technique in stabilized laboratory conditions

DAVOR PAVUNA
Department of Physics, University of Leeds, Leeds, UK

The results of extensive studies on the production of metallic glass ribbons by a single jet chill-block melt-spinning technique in laboratory conditions are summarized with emphasis on the data of practical importance. A device that stabilizes quenching conditions by surrounding the melt puddle with an atmosphere of He gas is described. The conditions for high stability are defined. The dependence of ribbon width and thickness on the volumetric flow rate, injection angle and substrate velocity are experimentally determined in such stabilized conditions. The cross-sectional geometric uniformity of the ribbons, analysed by Talysurf, is shown to be comparable with those produced by commercial laboratories, and/or within specially constructed chambers.

1. Introduction

Within the last few years most metallic glasses have been produced by the chill-block melt-spinning (CBMS) technique [1]. This involves squirting a jet of molten alloy onto the rim of a rotating roller and so obtaining lengths of ribbons. Because of the current scientific and technological importance of these materials, numerous authors have studied the influence of the CBMS processing parameters on the ribbon geometry and its cross-sectional uniformity [2–6], and have suggested various improvements of the basic technique [7, 8].

At the time of the third International Conference on Rapidly Quenched Metals when this work was begun, it was already known that the shape and the stability of the melt puddle [5, 6], as well as the surrounding atmosphere [7], have a major influence on the ribbon geometry and geometrical uniformity; also the first ribbons wider than 1 inch had already been produced [9].

Nevertheless, straightforward application in this laboratory of the CBMS principles as presented in the existing literature resulted not in a ribbon but only in a display of fireworks. This happened more than once until we learned the "know-how" that was not presented in the literature. Subsequently we developed two further improvements of the CBMS technique—the quenching stabilizer [8] and the low-temperature melt-spinning device [10].

In this paper most of the experimental data on the production of metallic ribbons by a single-jet-CBMS technique at room temperature are summarized. In the experimental part of the paper the objective has been to present data of practical importance rather than those of purely academic interest. I believe that this may be of help to the numerous newcomers in the field and at the same time a challenge to the other researchers, whose "know-how" has been unpublished and/or protected by various patents.

In the results an improved version of the quenching stabilizer [8] and the optimal conditions for its use are described. The dependence of ribbon geometry (width, thickness) and uniformity on the production parameters are also presented: volumetric flow rate, $500 < Q < 7000$ $mm^3\ sec^{-1}$, injection angle, $75° < \alpha < 90°$ and roller surface velocity, $18 < v_s < 50$ $msec^{-1}$ for various orifice diameters, $0.40 < \phi < 1.85$ mm (corresponding distances from the roller were, $h \simeq 4\phi$). The alloys studied were $Cu_{100-x}Zr_x$ (with x between 26 and 72.7 at%) and some other binary alloys. Finally, the cross-sections of some of the ribbons produced in stabilized conditions

0022–2461/81/092419–15$03.50/0

are presented and compared with original Metglas®* and requenched Metglas alloys in order to show the advantages of the quenching stabilizer.

2. Experimental procedures

2.1. Optimal production conditions

There are three major conditions that should be satisfied in order to ensure successful laboratory production of glassy alloy ribbons by the single-jet-CBMS technique in air at room temperature:

(1) Volumetric flow rate, Q, through the orifice of the crucible should be kept practically constant during the production procedure.

(2) The melt puddle should be maintained stable and protected from the turbulence (and dust, dirt etc.) caused by the rotating roller.

(3) The surface of the roller should be carefully polished and cleaned to ensure good thermal and mechanical contact with the melt puddle.

If these conditions are satisfied then by choosing the *optimal combination* of orifice diameter, ϕ, injection angle, α, injection gauge pressure, P, roller surface velocity, v_s, length of the nozzle, l_N, and substrate–orifice distance, h, for any particular master-alloy composition, one can expect to produce a ribbon. All this may, however, be insufficient and one then has to consider some of the following factors; superheating, the right time of applying the pressure if melting is controlled visually, the inner shape of the crucible, the optimal material for the roller surface, the collection of the ribbon while flying off the roller, the formation of a temperature gradient in the nozzle region of the crucible (resulting in a blocked nozzle), the shape and diameter of the induction heater, the vibration of the roller and many others.

Supposing that the optimal conditions are achieved, then a volumetric flow rate Q through the orifice of the crucible (controlled by the injection pressure P), will form a melt puddle out of which "flows" a ribbon at the (usually assumed) same volumetric flow rate, Q,

$$Q = A_R \cdot v_s = W \bar{t} v_s \qquad (1)$$

where A_R is cross-sectional area of the ribbon, and W and $\bar{t}$ are ribbon width and average thickness, respectively.

In practice, one is often faced with the fact that the volumetric flow rate through the nozzle, $\vec{Q}_N$, is somewhat greater than the actual in-flow into the ribbon, $\vec{Q}_R$

$$Q_N = |\vec{Q}_N| \gtrsim |\vec{Q}_R| = Q_R. \qquad (2)$$

This is caused mainly by the instabilities of the melt puddle and results in a number of molten droplets all over the laboratory. As emphasized in Equation 2, volumetric flow rates are actually *vector* quantities

$$\vec{Q}_N \neq \vec{Q}_R; \qquad \frac{\vec{Q}_N \cdot \vec{Q}_R}{Q_N Q_R} \neq 1. \qquad (3)$$

Surprisingly, introduction of "vector flows" into CBMS process analysis does not complicate the analysis; on the contrary, as will be seen, it gives a simple insight into the changes of the ribbon geometry with processing parameters.

If the injection angle, $\alpha = 90°$ (a jet perpendicular to the surface at the crest of the roller), the width of the ribbon depends primarily on the (vertical) flow rate Q_N (for a given v_s) and is practically independent of any losses of droplets from the puddle (which often occur for $\alpha = 90°$); the thickness depends mainly on the substrate velocity, v_s, i.e. the rate of horizontal in-flow of the material into the ribbon. Thus the instabilities mentioned above ($Q_R \lesssim Q_N$) are a major cause of the oscillations [11] of the ribbon thickness, t, along the length. Most of the previous studies of how the ribbon geometry depends on the CBMS process parameters were carried out under experimental conditions which were of importance theoretically but of less practical use.

For injection angles $\alpha < 90°$, the melt puddle is usually [5, 6] more stable; the horizontal inflow of the material into the ribbon is "smoother" so that $Q_N \simeq Q_R$ and the ribbon is more uniform in both longitudinal and transverse cross-section. The width depends primarily on the normal component of the flow rate (see Fig. 1) $Q_{NN} = Q_N \sin\alpha$ and is reduced by a factor $\sin\alpha$ compared to the width obtained in the $\alpha = 90°$ condition (with Q_N and v_s the same).

On the other hand the thickness increases because of the lengthening of the melt puddle [5]. This in turn is caused by the horizontal component of the vector flow, $Q_{NS} = Q_N \cos\alpha$. Vector flow analysis, together with some additional assumptions about the viscosity of the melt and/or minimum flow rate [2], can be used to make some predictions about the geometry of the ribbon [12], but such an analysis goes beyond the scope of this paper.

* Metglas® is a trademark of the Allied Chemical Corporation.

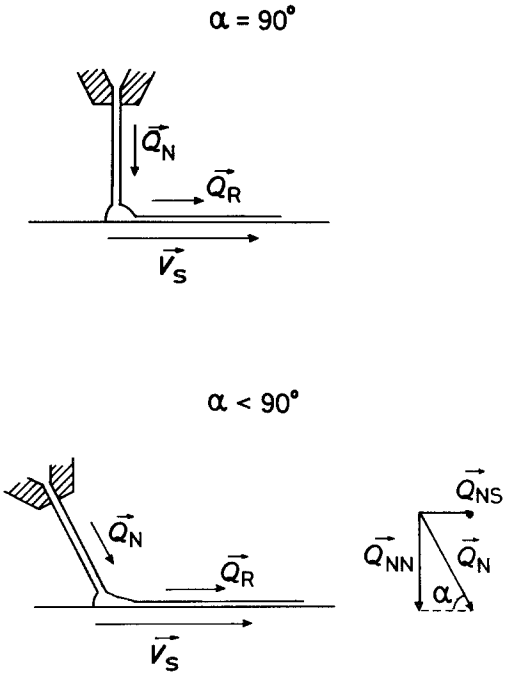

Figure 1 Schematic representation of the splitting of the "normal" volumetric flow rate, $Q_N(\alpha = 90°)$ into two components: $Q_{NN} = Q_N \sin\alpha$ and $Q_{NS} = Q_N \cos\alpha$ ($\alpha < 90°$). Note the slight lengthening of the melt puddle in case $\alpha < 90°$.

2.2. CBMS apparatus

Laboratory production equipment should be assembled from those elements which enable one to satisfy all reasonable combinations of processing parameters and, if necessary, quickly replace any of them. Usually it consists of a crucible surrounded by an induction heater coil suitably mounted just before the crest of the rotating roller. To this "standard" equipment a quenching stabilizer [8] has been added in the gap between the coil and the roller surface (see Fig. 2).

Two sets of apparatus have been tested for room-temperature CBMS (see Fig. 2) and also a low temperature apparatus [10] in order to achieve optimal production conditions for various glass forming materials and in attempts to quench polymers, pure Si, pure Ni, Cu–Li and some other materials.

The following is a summary of our experience with various elements of the production equipment constructed in our laboratory.

2.2.1. Crucible and induction heater

The role of the crucible is to ensure a steady flow of molten alloy through the nozzle onto the roller. Also, it should be able to withstand sudden rapid

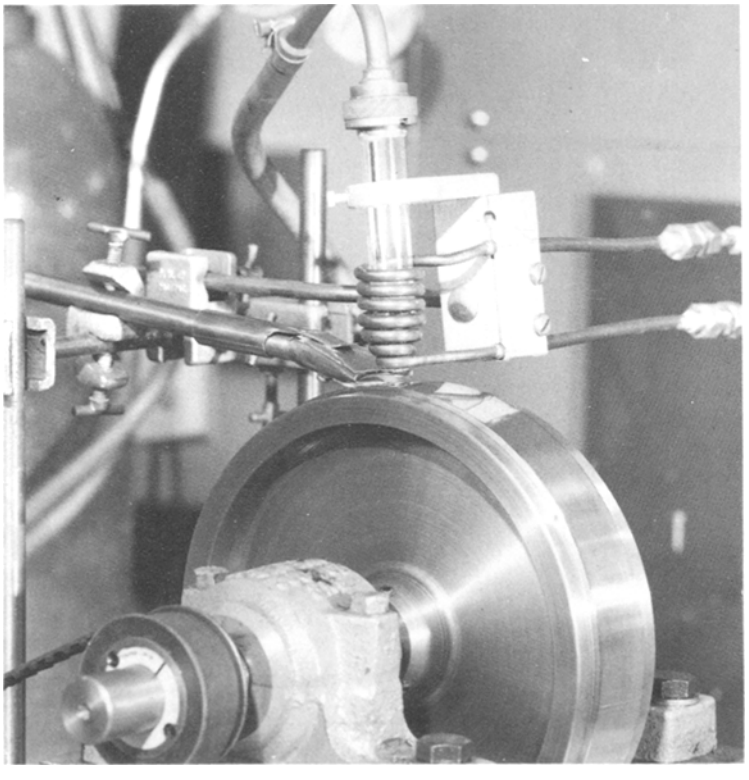

Figure 2 Photograph of the CBMS apparatus with quenching stabilizer mounted in the gap between the induction coil and rotating roller surface.

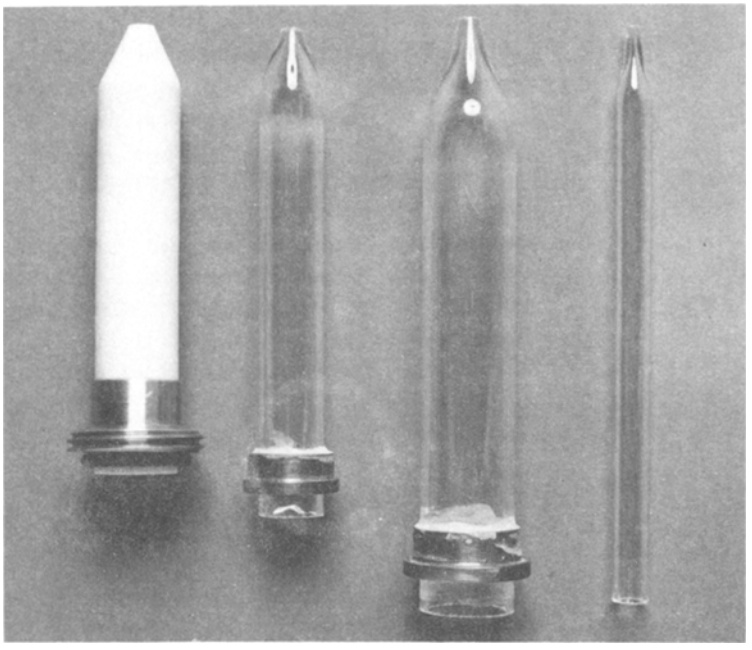

Figure 3 Photograph of three silica crucibles (inner diameters 5, 15 and 9 mm) and one alumina crucible (10 mm inner diameter).

changes in temperature and be capable of surviving several successful runs.

Three silica crucibles and one alumina crucible have been tested (see Fig. 3). Silica crucibles of inner diameters 5, 9 and 15 mm were hot drawn and then cut with a diamond saw in order to obtain a range of orifice diameters from 0.40 to 1.85 mm. The nozzle geometry was selected to minimize the contraction in the cross-sectional area of the molten jet as it leaves the nozzle orifice [11]; i.e. the nozzle–substrate separation, h, was always greater than two jet diameters, and typically $h \approx 4\phi$; the length of the nozzles was short, typically $\approx 2.5\phi$. Alumina crucibles were made by making a mould of the inner shape of the crucible, surrounding it with alumina powder and then applying a high pressure ($P \sim 140$ MPa) to the powder. The nozzles were then drilled and the crucible baked for 12 h at 800° C.

As the alumina crucible is non-transparent, a periscope tube [10] was added to it in order to enable observation of the process of melting and to apply the helium injection pressure at the desired moment. For different sizes of crucible, different induction coils were used. The coils were made of hollow copper tubing, wound anticlockwise and shaped to converge around the nozzle region of the crucible (see Fig. 2). This may cause levitation [13] of the alloy when strong ferromagnetic alloys are quenched (e.g. some Co-based systems) but can be recommended otherwise.

2.2.2. The rotating rollers

Six rollers of the following diameters and materials were tested: 200 mm mild steel roller; 206 mm mild steel roller with a shrunk on copper annulus (3 mm) (see Fig. 2); 206 mm duralumin roller with a shrunk on copper annulus (3 mm); 108 mm mild steel roller with a shrunk on copper annulus (4 mm); 100 mm bras roller with a shrunk on copper annulus (3 mm).

All of the rollers, except the brass one, were driven by a variable speed motor (0 to 2000 revs min^{-1}) via a tooth belt. Cog-wheel ratios of 3:1 and 6:1 made it possible to vary the surface velocities continuously from 10 to well over 60 $msec^{-1}$. The speed of the roller was measured by a stroboscope and was varied in steps of 5 $msec^{-1}$.

The 100 mm brass roller was a specially constructed turbine-roller [10] that has 32 buckets at each side which permits rotation (like a turbine) by means of air, an inert gas or liquid nitrogen vapour through two jet nozzles that are mounted on either side with jets directed into the buckets. The most satisfactory results were obtained with copper surfaces, particularly in the case of binary metal–metal systems, regardless of the material of the underlying roller. The copper surface is mechanically soft and has to be carefully polished

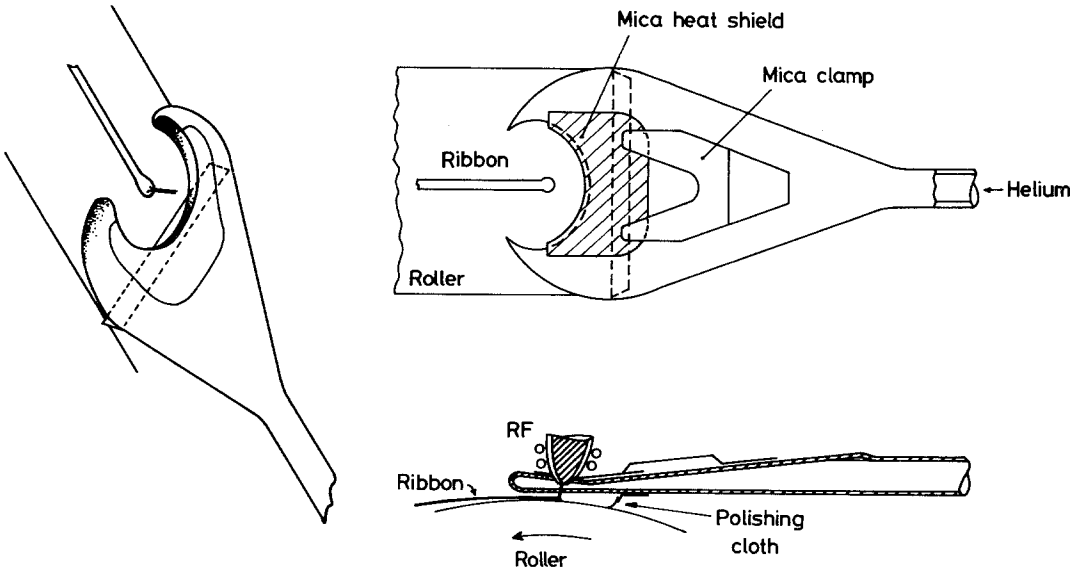

Figure 4 Schematic drawings of the improved model of the quenching stabilizer. Note the specific design of the "jaws" surrounding the melt puddle.

and cleaned; moreover, it was also cleaned with ether just before a production run. In our experience chromium and mild steel surfaces can also give very good results. It seems that careful preparation of the surface plays a more important role (at least at room temperature) than the actual material of the surface itself. Overall, the large diameter rollers seem to be the better experimental choice. To achieve a certain surface velocity one has to rotate the rollers at a smaller number of revs per min and this introduces vibrations at lower frequencies than with the smaller roller; these frequencies are below the high frequency vibrations of the melt puddle and have no influence on the ribbon geometry and uniformity. Also, in some cases the ribbon remains in contact with the surface for a whole revolution and, in the case of a small roller, may hit the puddle from the back, thereby disrupting the quenching process.

2.2.3. The quenching stabilizer

In order to achieve stable conditions when quenching in air at atmospheric pressure an additional device, the quenching stabilizer [8] was developed. It is a brass tube expanded into a "jaws" shaped opening (see Fig. 4) that surrounds the melt puddle. A polishing cloth underneath polishes the roller and, at the same time, deflects the draught of the roller. The flow of helium gas through the "jaws" surrounds the puddle during the quenching procedure, speeds up the cooling process and protects the alloy that is "flowing out" of the puddle from contamination by air.

The mica shield, clamped at the upper side of the stabilizer, protects the roller from heat during extensive runs and isolates the induction coil from the brass stabilizer.

Three models of quenching stabilzer were tested (see Figs 2 and 4) and the final version presented in Fig. 4 gives the best results. The shape of the "jaws" (4 mm in height) is designed to ensure maximum helium flow behind the puddle where the solidified ribbon (still hot and reactive) flows out along the surface. In the central area the opening is very narrow ($\sim$ 1 mm) so that direct helium flow does not destabilize the melt puddle.

Of course, the helium flow must not be too fast (i.e. not $> 1/20$ gauge pressure* for the old model, not $> 1/10$ gauge pressure for the jaws model because that can destabilize the melt puddle and hinder the process of rapid quenching. We have studied the behaviour of the melt puddle surrounded by the helium flow from the stabilizer by means of high-speed motion pictures and observed that *the primary condition for the successful application of the quenching stabilizer is a constant flow rate of the molten alloy,* Q_N. The stabilizer cannot improve the instabilities of the puddle caused by the fluctuations in flow rate,

* i.e. the gauge pressure used to provide the injection impetus for the melt.

but if Q_N is optimal (for the particular v_s) and the flow through the stabilizer is adjusted at about one twentieth of the gauge pressure (for the new model), stabilized production conditions are achieved. These conditions are then equivalent to the production conditions achieved within a reduced pressure chamber containing helium gas [7].

Use of inert gases, other than He, cannot be recommended because only He has the desired effect on the ribbon quality regardless of the ambient pressure (see Fig. 2 of Liebermann [7]); this point is of the highest importance when quenching in air at atmospheric pressure.

2.3. Experimental details

The master alloys were prepared by a standard metallurgical procedure described elsewhere [1]. Usually one large lump was prepared and then broken into smaller pieces. In order to ensure stable flow, a single piece only was used for a particular run. One can put more lumps into the crucible but then one has to ensure that they melt at the same time and create a continuous, stable flow after the injection pressure is applied; otherwise, an unstable flow might result, giving a few non-uniform ribbons and/or a short ribbon and a display of fireworks. In our experience, whenever quenching non-commercial materials in the laboratory, it is well worth using a single, sometimes very large (40 g) piece of master alloy.

The injection pressure was applied at the moment when the alloy was observed to be fully molten ($T \simeq T_m$). The resulting ribbon was somewhat non-uniform at the very beginning (~ first metre), and gradually narrower towards the end (~ last few metres). The remaining, typically, 10 to 20 metres were very uniform, i.e. the width and thickness were practically constant. This length of the ribbon was used for the geometrical measurements and the analysis of the run, while the very beginning and ends of the ribbons were discarded. The width of the ribbon was measured by a travelling microscope; the average thickness was calculated by dividing the ribbon mass by the density, length and width.

Maximum ribbon thickness was measured using a micrometer and, together with a number of ribbon "cross-sections" obtained by a Talysurf surface measuring instrument [8, 13], it was possible to compare the cross-sectional uniformity of the ribbons produced in various runs.

The injection angle, α, and the orifice–roller separation were always carefully adjusted before the run. A suitably constructed holder (see Fig. 2) made it possible to make very fine adjustments of these parameters.

The quenching process was also filmed by high-speed photography (1500 frames sec^{-1}) and the individual photographs, similar to those presented by other researchers [5, 6], were used for the study of the behaviour of the melt puddle in stabilized (and also non-stabilized) conditions.

The He flow through the quenching stabilizer was supplied from a separate He cylinder and controlled by a separate gauge. In some experiments, however, the stabilizer was connected onto the same cylinder that was used as the injection pressure supply. In such an arrangement only a fraction (~ one twentieth) of the injection pressure was let through the stabilizer branch of the system.

As most of the experiments were carried out in air at atmospheric pressure, hot ribbon that was flying off the roller was collected in an asbestos blanket. Otherwise pieces of the still reactive ribbon may catch on the metal parts of the equipment and burn and/or collect dust or dirt.

It is useful to emphasize that although the actual run lasted typically a second or two, each experiment was prepared for hours and if it worked well, a series of runs was conducted under the same conditions changing only one parameter at a time. This resulted in a high reproducibility of the results of our quenching experiments which is often difficult to achieve otherwise.

3. Results

The results of the measurements of the dependence of the ribbon geometry (W and $\bar{t}$) on the volumetric flow rate ($Q = Q_N$) can be summarized in two sets of data:

–"low Q" data (Q up to 4 $cm^3\ sec^{-1}$; $\phi \lesssim$ 1 mm);

–"high Q" data (Q up to 7 $cm^3\ sec^{-1}$; $\phi \gtrsim$ 1 mm).

Although this division might seem somewhat artificial, it is justified in the case of CBMS in stabilized laboratory conditions. It not only divides the results of separate series of experiments and enables easier presentation and analysis of the experimental data but, as will be shown, also defines two somewhat different production modes (see Section 4).

TABLE I $v_s = 20\ \text{msec}^{-1}$; $\alpha = 83° \pm 1°$

System	ϕ (mm)	Q (mm^3 sec^{-1})	$\bar{t}$ (μm)	t_{mic} (μm)	W (mm)	P_{QS} (kPa)
$Cu_{60}Zr_{40}$	1.06	602	28.7	37	1.05	0.5
		1 018	32.8	44	1.55	0.7
	0.80	664	32.6	38	1.02	0.5
		742	32.3	38	1.15	0.7
		1 360	36.8	50	1.85	1.7
		1 488	35.4	50	2.10	2.0
		1 690	34.1	45	2.48	2.5
		1 776	36.3	44	2.45	2.8
		1 870	35.3	45	2.65	3.5
		2 172	35.6	52	3.05	4.2
$Cu_{66}Ti_{34}$	0.98	754	36.3	44	1.04	0.8
		1 328	36.1	45	1.84	1.5
		1 500	37.9	50	1.98	2.0
		1 546	38.1	48	2.03	2.0
	1.03	1 190	33.6	39	1.77	1.5
		1 322	33.9	41	1.95	1.8
		1 408	33.5	48	2.10	1.8
		1 448	32.2	40	2.25	2.0
		1 714	38.1	45	2.25	2.7
		1 750	35.0	45	2.50	2.8
		1 930	35.7	48	2.70	3.5

3.1. "Low Q" data

The results of the "low Q" experiments are presented in Tables I and II and summarized in Fig. 5.

The roller surface speeds were 20 and 30 msec^{-1} and the injection angle was fixed at $83° \pm 1°$. These are roughly the production conditions suitable for the production of the best known glass-forming alloys. Of course, the injection angle could be smaller ($\alpha \approx 75°$) and the substrate speed, v_s, could be somewhat greater ($v_s > 30$ msec^{-1}), but the combination of the parameters used in our investigation is fairly representative. The main reason binary Cu–Zr and Cu–Ti were used as master alloys was that an enormous amount of these amorphous materials (a few hundred grams of very uniform ribbons) was needed for inelastic neutron-scattering experiments [14]. Furthermore, earlier investigations published by

TABLE II $v_s = 30\ \text{msec}^{-1}$; $\alpha = 83° \pm 1°$

System	ϕ (mm)	Q (mm^3 sec^{-1})	$\bar{t}$ (μm)	t_{mic} (μm)	W (mm)	P_{QS} (kPa)
$Cu_{66}Ti_{34}$	0.91	685	25.1	33	0.91	0.6
		1 236	28.0	35	1.47	2.0
		1 248	27.7	35	1.50	2.0
	0.98	2 033	30.1	40	2.25	4.0
		2 433	29.0	40	2.80	4.2
		2 487	29.1	42	2.85	4.2
		2 590	28.6	41	3.02	4.3
		2 691	28.9	41	3.10	4.4
	1.03	2 130	26.8	37	2.65	3.0
		2 178	26.9	37	2.70	3.0
		2 601	31.0	38	2.80	3.5
		2 676	31.3	38	2.85	3.5
$Cu_{60}Zr_{40}$	0.70	1 929	27.1	34	2.37	4.2
		1 947	26.0	33	2.50	4.2
		2 106	26.5	34	2.65	5.0
		2 166	25.7	34	2.81	5.0
$Cu_{27}Zr_{73}$	1.06	1 977	24.1	32	2.75	3.5
		2 523	28.5	37	2.95	3.5
		3 210	27.4	37	3.90	3.5
		3 635	30.0	38	4.04	3.5

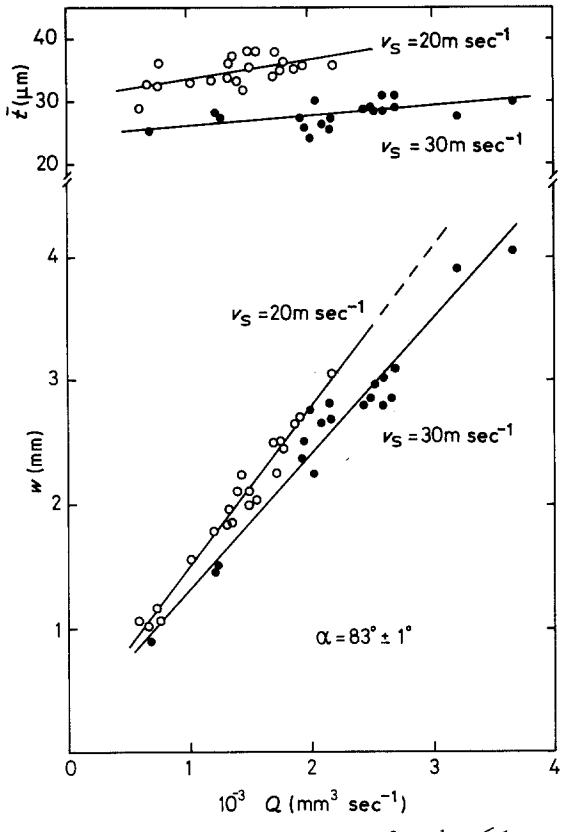

Figure 5 "Low Q" data (Q up to 4 cm^3 sec^{-1}; $\phi \lesssim 1$ mm; $\alpha = 83° \pm 1°$): ribbon width and average thickness against volumetric flow rate for Cu–Zr and Cu–Ti alloys produced in stabilized laboratory conditions (see Tables I and II for details).

other researchers were mainly concerned with technologically more interesting metal–metalloid systems, like Fe–Ni–B, Fe–B, Fe–Ni–P–B.

The experimentally obtained *linear* dependence of the ribbon width and average thickness on the volumetric flow rate (see Fig. 5) basically confirms similar results obtained by other researchers [1, 2] with Fe–Ni–B systems, and therefore indicates that the use of the quenching stabilizer in the "standard" CBMS process produces essentially the same results as would be obtained by CBMS within partly evacuated chambers [2, 7, 8].

As can be seen from Fig. 5, the ribbon width is a very weak function of the roller speed, v_s, and depends primarily on the normal component of the flow rate, Q_{NN}. (Note that in this case $\alpha = 83°$, i.e. the jet is "practically perpendicular" to the roller surface, so that $Q \simeq Q_N \simeq Q_{NN}$.) On the other hand, the average ribbon thickness, $\bar{t}$, is a weak function of the flow rate, Q, but depends strongly on the roller speed; so much so, that by determining the ribbon thickness one can usually re-establish what roller speed was used for the production of that particular ribbon.

The He flow through the quenching stabilizer was adjusted at 1/20 of the injection pressure, but the $Cu_{27}Zr_{73}$ runs (see Table II; $\phi = 1.06$ mm) were conducted with P_{QS} constant at 3.5 kPa while the injection pressure, P, was raised in steps of 7 kPa. This did not produce any change in the ribbon geometry from that obtained with the standard pressure $P_{QS} = (1/20)P$. Also, it did not result in any worsening of the quality (visual and geometrical uniformity) of the ribbon. This indicates that the pressure through the stabilizer, P_{QS}, is not a crucial parameter as regards the ribbon geometry as long as the other CBMS parameters are kept optimal for the particular master alloy. However, this was the case only when the newly designed stabilizer (see Fig. 4) was used. It has a wide polishing cloth underneath that stops the turbulence and creates an underpressure around the melt puddle so that practically any He flow through the "jaws" is good enough to ensure stabilized conditions. Nonetheless, the best results were always obtained with $P_{QS} \simeq (1/20)P$ and roller speeds of 30 ± 10 msec^{-1}.

The widest ribbon produced in the "low Q" mode was 4.04 mm wide ($\phi = 1.06$; see Table II and Fig. 5) for $Q = 3\,635$ mm^3 sec^{-1}. One can increase the injection pressure further and create flow rates higher than 4 cm^3 sec^{-1} but these require higher roller speeds ($v_s > 30$ msec^{-1}) in order to maintain a cooling rate of typically $\sim 10^6$ Ksec^{-1} which is necessary and usually sufficient for the production of most "standard" glass forming alloys. This, in turn, does not result in any particular increase of the ribbon width, which usually "saturates" at about $W_{max} \simeq 4\phi$ (see [1, 2]). For the production of even wider ribbons one should develop the multi-jet techniques [6, 15] and/or planar casting [15] that are usually used for the commercial production of wider ribbons.

3.2. "High Q" data

Instead of developing multi-jet techniques and/or planar casting we have tested the possibility of the production of wider ribbons (typically 5 mm) in the "high Q" mode (Q up to 7 cm^3 sec^{-1}) with large orifice diameters, 1 mm $\lesssim \phi < 2$ mm. In our opinion the ribbon of about (5 ± 2 mm) × (30 ± 5 μm) ($\bar{t}$) should be sufficiently wide and "bulky" for, at any rate, most scientific purposes.

TABLE III $v_s = 20$ msec^{-1}; $\alpha = 83° \pm 1°$

System	ϕ (mm)	q Q (mm^3 sec^{-1})	$\bar{t}$ (μm)	t_{mic} (μm)	W (mm)	P_{QS} (kPa)
$Cu_{60}Zr_{40}$	1.05	598	28.5	36	1.05	0.4
		1 024	30.0	38	1.70	0.6
		1 780	36.3	44	2.45	2.9
		3 440	43.0	58	4.01	3.5
$Cu_{66}Ti_{34}$	1.03	2 670	42.4	59	3.15	3.2
$Cu_{27}Zr_{73}$	1.44	4 056	48.9	65	4.15	4.0
		4 495	47.8	64	4.70	4.2
		4 620	46.2	66	5.00	4.4
		4 890	46.6	68	5.25	4.5
		5 159	52.0	68	5.02	5.2
		5 324	49.2	65	5.41	5.2
		5 612	51.0	67	5.52	5.6
	1.55	5 410	53.0	70	5.10	5.5
		6 004	53.1	71	5.65	5.7
		6 154	50.9	69	6.05	5.8

Such ribbon dimensions are also very suitable for the measurements of some transport properties, for instance, the Hall coefficient of non-ferromagnetic binary alloys [16]. This was the reason why Cu–Zr and Cu–Ti systems were mostly quenched in these experiments.

The results of "high Q" experiments are presented in Tables III to VI and summarized in Figs 6 and 7.

The roller surface speeds were 20 and 30 msec^{-1}; the injection angles 83° ± 1°, 76° ± 1° and ~ 90°; the roller–orifice separation was always ~ 4ϕ.

It can be seen from Fig. 6 that neither W nor $\bar{t}$ are linear functions of Q. As in the "low Q" mode the width depends primarily on the flow rate, but here the relation is more complex; data analysis yields $W \propto Q^{0.75}$ with v_s = constant and $\alpha = 83°$. On the other hand the average ribbon thickness is much more dependent on the flow rate ($\bar{t} \propto Q^{0.25}$) than in the "low Q" mode, where it was nearly constant (for any given v_s). This could be understood as a direct consequence of the use of large orifice diameters: the greater the diameter, the longer the melt puddle and the thicker the ribbon ($\bar{t} \propto l^{1.6}$ for $\alpha = 90°$ [5]). In these experiments with $\phi \approx 1.4$ to 1.5 mm with $\alpha = 83°$, the length of the puddle, l, is also slightly lengthened by the horizontal component of the vector flow, $Q_{NS} = Q_N \cos \alpha$ (see Section 2.1).

The effect of the increase of the average thickness caused by the use of larger orifices could also, together with the mass conservation law ($Q = W \cdot \bar{t} \cdot v_s$), partly account for lower W readings at very high values of Q.

Another effect that partly accounts for both higher $\bar{t}$ and lower W readings is the formation of the edge shoulders [8] that are probably caused by the "hydraulic jump effect" [11, 17] (see also

TABLE IV $v_s = 30$ msec^{-1}; $\alpha = 83° \pm 1°$

System	ϕ (mm)	Q (mm^3 sec^{-1})	$\bar{t}$ (μm)	t_{mic} (μm)	W (mm)	P_{QS} (kPa)
$Cu_{66}Ti_{34}$	0.90	680	24.6	33	0.92	0.8
		1 250	26.9	38	1.55	2.2
$Cu_{45}Zr_{55}$	1.18	1 992	28.9	42	2.30	4.3
		2 243	29.9	42	2.51	4.4
	1.10	3 312	33.1	45	3.34	5.5
		3 696	35.2	46	3.50	5.7
$Cu_{60}Zr_{40}$	1.55	2 494	29.2	40	2.85	4.2
$Cu_{27}Zr_{73}$	1.44	4 270	37.5	48	4.10	5.0
		5 052	35.5	52	4.75	5.4
		5 863	38.3	50	5.10	6.0
		6 186	40.0	52	5.15	6.3
		6 447	40.7	55	5.28	6.6
		6 662	40.7	54	5.45	7.2

TABLE V $v_s = 20$ msec^{-1}; $\alpha \simeq 90°$

System	ϕ (mm)	Q (mm^3 sec^{-1})	$\bar{t}$ (μm)	t_{mic} (μm)	W (mm)	P_{QS} (kPa)
$Cu_{60}Zr_{40}$	1.36	4 590	42.9	60	5.72	4.0
		5 502	44.0	65	6.25	5.0
	1.60	4 344	41.0	62	5.29	3.8
		4 548	41.9	62	5.50	4.0
		6 718	50.1	70	6.71	6.0
		6 812	50.0	67	6.85	6.1

Sections 3.3 and 4 and Fig. 8). On the basis of the results presented in Fig. 6 one would expect that, with α held at a value of 83°, experiments with $v_s = 25$ msec^{-1} would result in $\bar{t}$ and W readings that lie in between the lines defined by $v_s =$ 20 and 30 msec^{-1}. Indeed, the readings obtained in several test runs conducted at $\alpha = 83°$ with v_s $= 25$ msec^{-1} confirmed that expectation.

If, however, we now change the injection angle α to a value of 90°, we find that with a value of $v_s = 20$ msec^{-1}, the $\bar{t}$ readings *also* lie in between these lines (see the upper part of Fig. 7 and Table V). Moreover, the change of the injection angle to a value of 76°, with v_s now being held at 30 msec^{-1},*also* yields practically the same $\bar{t}$ against Q plot (see upper part of Fig. 7 and Table VI). In other words, a change in injection angle, α, of about 7° can, as far as average thickness is concerned, be exactly compensated by a change in the surface velocity of the roller, v_s, of about 5 msec^{-1}.

Before calling these observations a scaling rule, one would have to test a much wider range of roller speeds and injection angles, but even so they can serve as a useful guideline to the experimentalist when preparing a new run with a somewhat different geometrical arrangement.

In the case of $\alpha = 90°$, the W readings were much closer to the hypothetical "linear line", so the maximum ribbon widths ($W = 6.85$ mm) were obtained. In such an arrangement the jet is perpendicular to the roller surfaces, so the fairly high total momentum of the vertical flow rate, $\vec{Q}_N$ (see Fig. 1) not only widens the melt puddle (and therefore the ribbon) but also creates a more distinct "hydraulic jump effect" [8, 17] (for detailed explanation see [11], section F: puddle stability). As a consequence, the transverse cross-sections (obtained by Talysurf) of all wider ribbons possess the "shoulders" at the edges [8] (see also Section 3.3). Again, that partly accounts for somewhat lower W readings at very high values of Q, e.g. the deviation from the linear W–Q relation.

The ribbons obtained for $\alpha = 76°$ and $v_s =$ 30 msec^{-1} were significantly narrower than those

TABLE VI $v_s = 30$ msec^{-1}; $\alpha = 76° \pm 1°$

System	ϕ (mm)	Q (mm^3 sec^{-1})	$\bar{t}$ (μm)	t_{mic} (μm)	W (mm)	P_{QS} (kPa)
$Cu_{27}Zr_{73}$	1.45	3 271	37.4	45	2.90	4.5
		3 422	39.6	48	2.89	4.6
		3 630	40.3	48	3.00	4.7
		3 891	41.7	50	3.11	4.8
		4 078	41.8	52	3.02	4.9
		4 100	42.7	56	3.20	5.0
		4 205	42.6	52	3.29	5.2
		4 550	43.3	50	3.50	5.4
$Cu_{45}Zr_{55}$	1.20	1 013	28.9	38	1.28	2.2
		1 759	30.8	42	1.90	2.5
		2 225	35.3	47	2.11	3.5
		2 710	39.3	50	2.30	4.0
		3 270	40.2	50	2.71	4.6
		3 555	42.0	55	2.82	4.8
	1.25	1 218	28.0	37	1.45	2.0
		1 787	30.4	42	1.94	2.8
		2 430	36.7	44	2.21	3.8
		3 025	39.5	52	2.55	5.2
		3 679	40.9	52	3.00	5.6

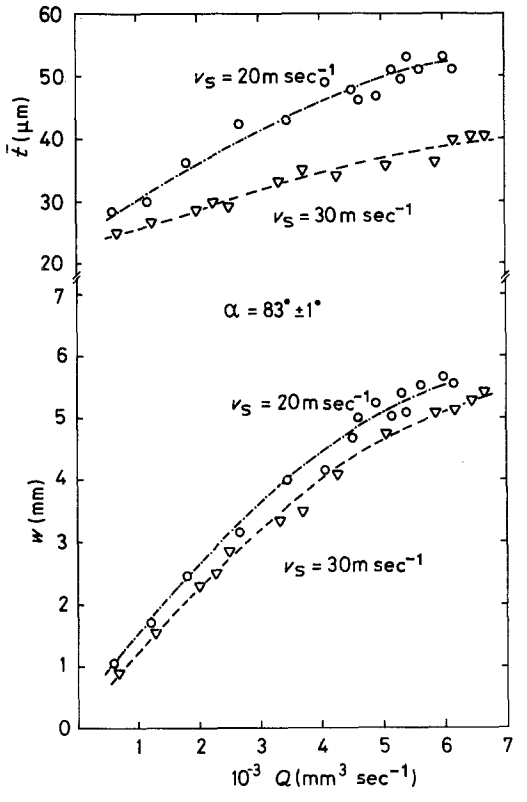

Figure 6 "High Q" data (Q up to 7 cm^3 sec^{-1}; $\phi \gtrsim 1$ mm; $\alpha = 83° \pm 1°$): ribbon width and average thickness against volumetric flow rate for Cu–Zr and Cu–Ti alloys produced in stabilized conditions (see Tables III and IV for details).

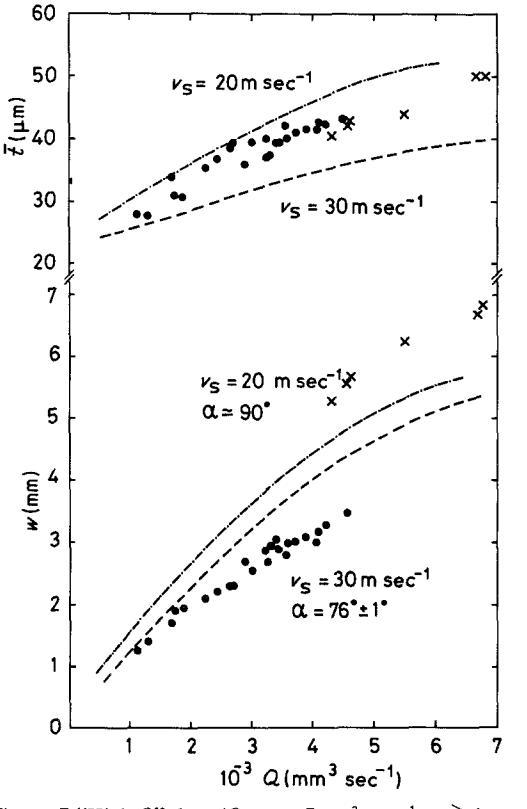

Figure 7 "High Q" data (Q up to 7 cm^3 sec^{-1}; $\phi \gtrsim 1$ mm; $\alpha = 76° \pm 1°$ and $\alpha \approx 90°$): ribbon width and average thickness against volumetric flow rate for Cu–Zr alloys produced in stabilized conditions (see Tables V and VI for details). The dotted lines represent the "high Q" data obtained for $\alpha = 83° \pm 1°$ (see Fig. 6).

produced for $\alpha = 90°$ and $v_s = 20$ msec^{-1} (see Fig. 7), but they were geometrically very uniform and this experimental arrangement is strongly recommended. It seems that $\alpha \simeq 75° \pm 3°$ is the optimal injection angle for the production of most glassy alloys as the puddle is very stable. However, for the production of the more difficult glass-formers like $Fe_{85}B_{15}$, higher roller speeds should be used in order to reduce the average thickness and thereby increase the cooling rate [4].

The pressure applied through the quenching stabilizer is reported in Tables III to VI for each particular run. As before, it was typically 1/20 of the injection pressure. Somewhat higher pressures can be (and were) used without any danger of hindering the quenching process. Moreover, at very high values of Q it is often desirable to apply higher He pressure through the stabilizer ($\sim 1/10$ P) in order to protect the enormous melt puddle that is formed.

The CBMS experiments at very high values of Q, with large orifices ($\phi \gtrsim 1.5$ mm) are very dangerous and plenty of experience and skill is needed in order to produce continuous ribbon rather than fireworks. It was observed that the temperature of the melt plays a very important role. It is crucial to apply the injection pressure at the right moment, when the alloy is fully molten ($T \approx T_m$). If the temperature of the melt is too high (some 100° C above the melting temperature) the ribbon becomes ragged and often burns (when quenched in air). The quenching stabilizer with $P_{QS} = (1/10)P$ *minimizes* these undesirable effects but cannot eliminate them completely.

3.3. The quality of the ribbons

The quality of the ribbon, e.g. its geometrical and visual uniformity, depends on the stability and shape of the melt puddle [5, 6] and the variation of the Newtonian coefficient of cooling along the ribbon–roller interface [11]. Therefore, one would expect that the CBMS in stabilized production conditions, as described in Section 2.2.3, should result in ribbons of very good visual appearance and geometrical uniformity.

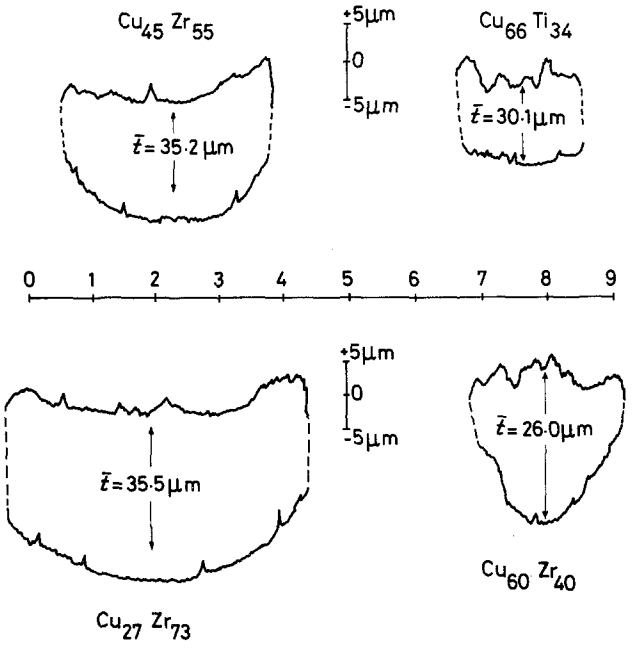

Figure 8 The transverse cross-sections of ribbons produced in stabilized conditions. The microprofiles were measured by Talysurf, surface measuring instrument. Note that specimen thicknesses are not drawn to scale.

Indeed, as has already been shown elsewhere [8] the use of the quenching stabilizer improves the cross-sectional uniformity of the ribbon.

The transverse cross-sections of all the ribbons were analysed by Talysurf, a surface measuring instrument, and in Fig. 8 some typical transverse cross-sections of the ribbons produced in either "low Q" ($Cu_{60}Zr_{40}$ and $Cu_{66}Ti_{34}$) or "high Q" modes ($Cu_{27}Zr_{73}$ and $Cu_{45}Zr_{55}$) are presented.

The important feature, common to all ribbons produced in stabilized conditions, is that the thickness variation along the length and across the width of the ribbon lies within ~ 25% (oscillation of ± 4 μm for the average ribbon thickness of ~ 30 μm). This is comparable with the thickness uniformity of commercial Metglas® and Vitrovac®* ribbons (see [8]) or of the ribbons produced in specially constructed evacuated chambers [7, 13]. For comparison, ribbons produced in air often show thickness oscillations of ~ 50% (± 7 μm in 30 μm). Another feature, common to all wider ribbons ($W \gtrsim 4$ mm), is the presence of two "ridges" at both edges of the "upper surface (see $Cu_{27}Zr_{73}$ cross-section in Fig. 8). These "edge shoulders" are most probably caused by the "hydraulic jump effect" (see [11] p. 834) and are difficult, if not impossible, to avoid whenever one attempts to produce wider ribbons by the single-jet-CBMS technique.

Although the transverse cross-sections of the narrower ribbons ($W \simeq 2 \pm 1$ mm) look at first glance more irregular than those of the wider ones, most of them are very uniform with thickness oscillations within 12% (± 2 μm in 30 μm; see $Cu_{66}Ti_{34}$ or $Cu_{60}Zr_{40}$ cross-sections in Fig. 8).

In order to show the advantages of the quenching stabilizer we melted some 50 metres of the commercially available Metglas® 2826 ribbon, and made a lump which we used as a "master-alloy" charge in the production run under stabilized conditions with the following parameters: $\phi = 0.74$ mm, $\alpha = 83°$, $v_s = 30$ msec^{-1}, $Q = 1\,525$ mm^3 sec^{-1}, $P_{QS} = 2.5$ kPa.

As a result we obtained a very uniform ribbon 1.84 mm wide and 27.6 μm thick ($\bar{t}$). The thickness uniformity was within ~ 18% (± 2.5 m in 27.6 μm). The transverse cross-section of this "requenched Metglas" ribbon is compared with the cross-section of the original Metglas® 2826 in Fig. 9. Not only are the cross-sections comparably uniform, but the ribbons are also visually similar; very shiny on the "upper" surface and matt on the "lower" one (that was in contact with the roller).

This test, as well as the other results, confirm that the use of the quenching stabilizer makes possible the production of ribbons of the highest quality under laboratory conditions.

* Vitrovac® is a trade mark of Vacuumschmelze GMBH.

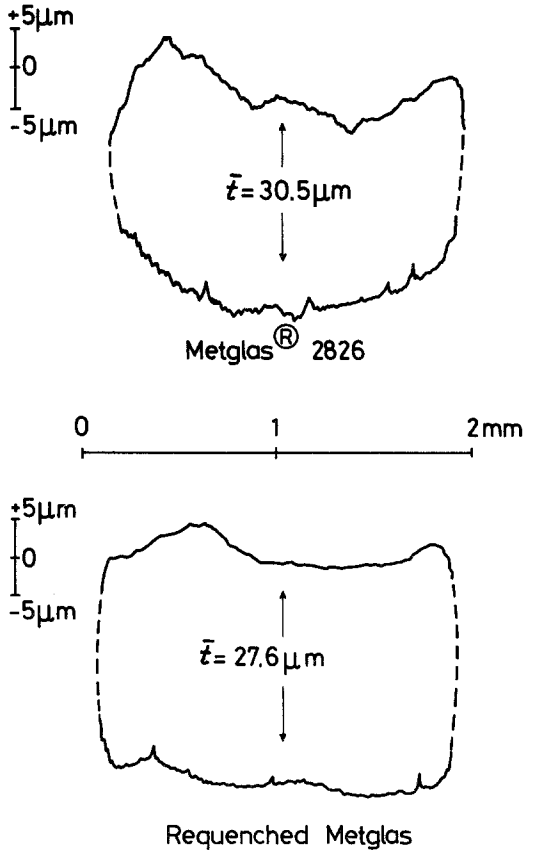

Figure 9 A comparison of the randomly chosen transverse cross-sections of commercial Metglas® 2826 ribbon and "requenched Metglas" ribbon produced in stabilized conditions (see Section 3.3). The ribbons also look very similar. Note that ribbon thicknesses are not drawn to scale.

4. Discussion

Various empirical relations have been established to predict ribbon width and thickness dependence on the CBMS process parameters [1–3, 5].

Kavesh [3] introduced two theoretical models and obtained the following relationships:

(1) Thermal boundary layer development

$$W = c\frac{Q^{0.75}}{v_s^{0.25}} \tag{4}$$

where c is a constant, and

$$\bar{t} = \frac{1}{c}\frac{Q^{0.25}}{v_s^{0.75}}. \tag{5}$$

(2) Energy equilibrium

$$W \text{ independent of } v_s \tag{6}$$

$$\bar{t} \propto \frac{1}{v_s}. \tag{7}$$

The experimental data of Liebermann and Graham [1] and of Allied Chemical Co. Laboratories [3] which Kavesh compared with the predictions of the models were not in a good agreement with either model. Instead somewhat different empirical relations were found

$$W = c'\frac{Q^{0.83}}{v_s^{0.17}} \tag{8}$$

where c' is a constant, and

$$\bar{t} = \frac{1}{c'}\frac{Q^{0.17}}{v_s^{0.83}}. \tag{9}$$

These give the best fit to the available experimental data. Kavesh [3] also suggested that the thermal boundary layer model provides a more complete framework for correlation and prediction of the ribbon dimensions and that Q, the volumetric flow rate, is the fundamental controlling parameter rather than the orifice diameter or the jet velocity separately.

Recently Liebermann [2] proposed the following relations between the ribbon dimensions and the controlling parameters

$$W = \phi + \frac{Q - Q_{\min}}{\nu_p}\left(1 - \frac{\beta}{2}\right) \tag{10}$$

and

$$\bar{t} = \frac{Q}{v_s W} = \frac{Q\nu_p}{\phi\nu_p + (Q - Q_{\min})[1 - (\beta/2)]} \tag{11}$$

where β is the injection angle in radians defined as $\beta = \pi/2 - \alpha$, $Q_{\min}$ is the flow rate required to produce the ribbon width equal to the orifice diameter ($W_0 = \phi$), while ν_p is an empirical constant, called the "dynamic melt puddle viscosity" [2]; typically $\nu_p \simeq 900$ to $1100\ \text{mm}^2\ \text{sec}^{-1}$ [2]. Although Lieberman developed Equations 10 and 11 on the basis of his experimental evidence and experience, they are consistent with Kavesh's theoretical conclusions, Equations 6 and 7; they therefore seem to represent an aspect of Kavesh's "energy equilibrium" model. Liebermann has found that his experimental results are consistent with Equation 10, i.e. that within the scatter of the experimental data there seems to exist a linear Q–W relationship, regardless of the type of ambient pressure in which CBMS is conducted. However, his experiments were conducted at relatively low values of Q: $Q \lesssim 2728\ \text{mm}^3\ \text{sec}^{-1}$

with $W \leqslant 2.8$ mm, $\phi = 0.66$ mm and $\alpha = 90°$ for casting in a He atmosphere; $Q \leqslant 3\,723$ mm^3 sec^{-1} with $W \leqslant 2.90$ mm, $\phi = 1.25$ mm and $\alpha = 70°$ for casting in air; only in the case of "vacuum" casting was Q up to 4798 mm^3 sec^{-1} with $W \leqslant 5.20$ mm, $\phi = 0.53$ mm and $\alpha = 90°$.

The results of our "low Q" experiments (see Section 3.1 and Fig. 5) seem to fit Liebermann's Equation 10 very well. With $\nu_p \simeq 965$ mm^2 sec^{-1} one can construct one linear $Q-W$ plot for the data corresponding to both $v_s = 20$ and 30 msec^{-1}. Two $Q-\bar{t}$ plots were then equally well reproduced by Equation 11.

The "non-linear", "high Q" data cannot be described by Liebermann's equations. The analysis of "high Q" data ($\alpha = 83°$; v_s = constant) yields: $W = kQ^{0.75}$ and $\bar{t} = (1/k)Q^{0.25}$, (where k is a constant) which is very similar to the prediction of Kavesh's thermal boundary layer model, i.e. Equations 4 and 5. (However, note that Kavesh assumed $\alpha = 90°$, while in our case $\alpha = 83°$.)

Therefore, it seems likely that the "energy equilibrium" type of model (Equations 6, 7, 10 and 11 and similar) could be successfully used at values of Q up to ~ 4 cm^3 sec^{-1} while a wider range of Q values and particularly "high Q" data ($Q > 4$ cm^3 sec^{-1}) could be successfully described in terms of the thermal boundary layer type of model (Equations 4, 5, 8, 9 and similar).

Liebermann's Equations 10 and 11, although quantitatively inaccurate at very high Q values, are of a great help to the experimentalist as they reveal the relation between all crucial experimental parameters Q, v_s, ϕ and α ($\beta = 90° - \alpha$). They are particularly useful for data analysis and enable one to develop a deeper understanding of the practical aspects of CBMS which are important in everyday laboratory practice.

5. Conclusions

Several conclusions can be made as a result of the extensive studies of the production of metallic glass ribbons by a single-jet-CBMS technique in stabilized laboratory conditions.

(1) The quenching stabilizer, a device that stabilizes quenching conditions by surrounding the melt puddle with an atmosphere of He gas, makes possible the production of ribbons of the highest geometrical uniformity and visual appearance.

(2) The geometrical uniformity of ribbons produced in stabilized conditions is within 25% (oscillations of $\pm 4\,\mu$m for the average ribbon thickness of about 30 μm), which is comparable with the geometrical uniformity of commercially available ribbons. Also, these ribbons are very similar to the commercial ones in appearance.

(3) The quenching stabilizer causes no direct, measurable changes in the ribbon geometry. The ribbon width is primarily controlled by the normal component of the volumetric flow rate, while the average thickness depends predominantly on the surface speed of the roller.

(4) The injection angle, α, influences both the width and average thickness. The increase/decrease of either the injection angle by about 7°, or the roller speed by about 5 msec^{-1} (with all other parameters unchanged), produces practically the same relative decrease/increase of the average ribbon thickness. The ribbon width changes accordingly, satisfying the mass conservation law, $W = Q/v_s \cdot \bar{t}$. This holds at least for $75° \lesssim \alpha \lesssim 90°$ and 20 msec^{-1} $\lesssim v_s \lesssim$ 30 msec^{-1}.

(5) The results of "low Q" experiments (Q up to 4 cm^3 sec^{-1}, $\phi \leqslant 1$ mm; $\alpha = 83° \pm 1°$) support Liebermann's empirically derived linear relation between volumetric flow rate, Q, and ribbon width, W.

(6) The "high Q" data (Q up to 7 cm^3 sec^{-1}; $\phi \gtrsim 1$ mm, $\alpha = 83° \pm 1°$) show more complex behaviour ($W \propto Q^{0.75}$; $\bar{t} \propto Q^{0.25}$; $v_s = 20$, 30 msec^{-1}) as predicted by Kavesh's thermal boundary layer model.

(7) Therefore, it seems that the "energy equilibrium" type of model ($W \propto Q$ and independent of v_s; $\bar{t} \propto v_s^{-1}$) can be successfully used only for Qs up to ~ 4 cm^3 sec^{-1} while a wider range of Qs and "very high Q" data ($Q > 4$ cm^3 sec^{-1}) in particular, can be successfully described in terms of thermal boundary layer model ($W \propto Q^{0.75} v_s^{-0.25}$; $\bar{t} \propto Q^{0.25} v_s^{-0.75}$).

Whether or not the quenching stabilizer could also be used successfully in multi-jet-CBMS techniques and/or planar casting is the subject of our present studies and the results will be presented elsewhere [12].

Acknowledgements

I am very grateful to Professor J. S. Dugdale for his constant interest, encouragement and help in all phases of creation of this paper. I am also grateful to Dr H. H. Liebermann (General Electric, USA) for numerous useful discussions and suggestions. I should also like to thank Mr M. Walker for the preparation of master alloys and experimental

assistance and Mr. D. Hainsworth for his invaluable technical help and assistance. Financial support from the Science Research Council is gratefully acknowledged.

References

1. H. H. LIEBERMANN and C. D. GRAHAM, JR, *IEEE Trans. Magn.* **MAG-12** (1976) 921.
2. H. H. LIEBERMANN, *Mater. Sci. Eng.* **43** (1980) 203.
3. S. KAVESH, "Metallic Glasses", (ASM, Metals Park, Ohio, 1978) p. 275.
4. H. A. DAVIES, "Rapidly Quenched Metals III", Vol. I, (The Metals Society, London, 1978) p. 1.
5. H. H .HILLMANN and H. R. HILZINGER, *ibid* (The Metals Society, London, 1978), p. 22.
6. J. L. WALTER, *ibid* p. 30.
7. H. H. LIEBERMANN, *ibid* p. 34.
8. D. PAVUNA, *J. Non-Cryst. Sol.* **37** (1980) 133.
9. T. R. ANTHONY and H. E. CLINE, *J. Appl. Phys.* **50** (1979) 245.
10. D. PAVUNA and D. HAINSWORTH, *J. Non-Cryst. Sol.* **37** (1980) 417.
11. T. R. ANTHONY and H. E. CLINE, *J. Appl. Phys.* **49** (1978) 829.
12. D. PAVUNA, to be presented at the 4th International Conference on Rapidly Quenched Metals, August, 1981, Sendai, Japan.
13. M. R. J. GIBBS, J. E. EVETTS and W. J. SHAH, *J. Appl. Phys.* **50** (1979) 7642.
14. T. M. HOLDEN, J. S. DUGDALE, G. C. HALLAM and D. PAVUNA, unpublished work (1980).
15. H. H. LIEBERMANN, *IEEE Trans. Magn.* **MAG-15** (1979) 1393.
16. B. L. GALLAGHER and D. GREIG, unpublished work (1980).
17. H. H. LIEBERMANN (General Electric, USA) personal communication (1980).
18. C. E. MOBLEY, "New Trends in Materials Processing", (ASM, Metals Park, Ohio, 1976), p. 128.

Received 6 January and accepted 11 February 1981.